JOURNAL OF THERMOPHYSICS AND HEAT TRANSFER
Vol. , No. ,

Blackout Analysis of Small Cone-Shaped Reentry Vehicles

Sahadeo Ramjatan*
University of Florida, Gainesville, Florida 32611
and
Thierry Magin,† Thorsten Scholz,‡ Van der Haegen Vincent,§ and Jan Thoemel¶
von Kármán Institute for Fluid Dynamics, 1640 Rhode-Saint-Genese, Belgium

DOI: 10.2514/1.T4825

The high temperatures associated with the hypersonic reentry process lead to an increase in the collisions between molecules, which may result in the disruption of the electronic structure, producing free electrons and ions. This production of free electrons and ions creates a plasma or ionized flowfield around the vehicle that is known to degrade the quality of radio-wave signal propagation, leading to a loss of communication or "blackout." This study involves performing hypersonic computational fluid dynamics simulations in the commercial software CFD++ with a blunt-nosed cone geometry at different flight conditions to predict how and when ground communication can be achieved to aid in the design of an alert transmitter, which is an extension of aircraft collision-avoidance system technology. Computational results show that a small blunt-nosed cone geometry has decreased ionization regions as the cone angle decreases due to a shifting of the reaction zone further downstream. As a result, higher freestream velocities have less of an impact in determining the location for an antenna, and communicating along the stagnation line is seen to be independent of cone angle.

Nomenclature

c	=	mass fraction
$\boldsymbol{E}$	=	electric field, N/C
E_k	=	kinetic energy, J
e	=	electron charge, 1.6×10–19 C
f_{link}	=	frequency band, Hz
f_p	=	plasma cutoff frequency, Hz
κ	=	correction factor
k	=	wave number
M	=	Mach number
m_e	=	electron mass; 9.1×10^{-31} kg
N_{e_o}	=	characteristic electron density in stagnation region as function of freestream velocity, cm^{-3}
$N_{e_{\text{peak}}}$	=	peak electron density, cm^{-3}
n_{cr}	=	critical electron density for a frequency band, m^{-3}
n_e	=	electron density, m^{-3}
$n_{\text{e/s}}$	=	electron density at stagnation point, m^{-3}
$n_{\text{e/w}}$	=	electron density at wake region, m^{-3}
P_G	=	pressure after shock wave, Pa
P_∞	=	freestream pressure, Pa
p	=	flowfield pressure, Pa
$\boldsymbol{q}$	=	heat flux vector, W/m^2
R	=	gas constant, $\text{J/(mol} \cdot \text{K)}$
R_n	=	nose radius, m
S	=	distance along the wall of the blunt-nosed cone, m
T	=	temperature, K
T_r	=	rotational temperature, K
T_t	=	translational temperature, K
u	=	velocity in x direction, m/s
V	=	freestream velocity, m/s
$\boldsymbol{V}$	=	flowfield velocity vector, m/s
$\boldsymbol{V}_l$	=	flowfield velocity vector of species i, m/s
v	=	velocity in y direction, m/s
$\dot{w}$	=	local rate of change of ρ_i, $\text{kg/(m}^3 \cdot \text{s)}$
x	=	distance along body, m
z	=	altitude, km
α	=	angle of attack, deg
γ	=	isentropic coefficient
ε	=	emittance
ε_o	=	permittivity in free space; 8.85×10^{-12} F/m
μ_0	=	permeability in free space; $4\pi \times 10^{-7}$ H/m
ρ	=	density, kg/m^3
ρ_i	=	density of species i, kg/m^3
σ	=	Stefan–Boltzmann Constant; 5.66961×10^{-8} $\text{W} \cdot \text{m}^{-2} \cdot \text{K}^{-4}$
τ_{xy}	=	stress in y direction exerted on a plane perpendicular to x axis, N/m^2
ω	=	angular frequency, rad/s
ω_p	=	plasma angular frequency, rad/s

Subscripts

i	=	species i
∞	=	freestream conditions

I. Introduction

THE reentry process is one of the most challenging aspects of the design phase for space missions. Due to reentry flight conditions, design constraints exist, including the material one can use due to the high temperatures encountered. In addition, the physical understanding and computational evaluation of the reentry flowfield including aeroheating computations are still being investigated. Performing experimental work to replicate flight scenarios can be difficult and expensive. Furthermore, high velocities on the order of magnitude of 7–11 km/s imply strong shock waves and extreme aerodynamic heating of the vehicle. These high temperatures result in an increase in collisions of the molecules, which may result in the disruption of the electronic structure,

Presented as Paper 2015-2081 at the 53rd AIAA Aerospace Sciences Meeting, Kissimmee, FL, 5–9 January 2015; received 3 August 2015; revision received 7 June 2016; accepted for publication 27 June 2016; published online XX epubMonth XXXX.

*Graduate Student, Mechanical and Aerospace Engineering; von Kármán Institute for Fluid Dynamics, Chaussee de Waterloo 72, 1640 Rhode-Saint-Genese, Belgium; sramjatan1@ufl.edu. Student Member AIAA.

†Assistant Professor, Aeronautics and Aerospace Department, Chaussee de Waterloo 72; thierry.magin@vki.ac.be. Member AIAA.

‡Ph.D. Student, Aeronautics and Aerospace Department, Chaussee de Waterloo 72; scholz@vki.ac.be.

§QARMAN Project Manager, Aeronautics and Aerospace Department, Chaussee de Waterloo 72; vdh@vki.ac.be.

¶QB50 Project Manager, Aeronautics and Aerospace Department, Chaussee de Waterloo 72; jan.thoemel@vki.ac.be.

producing free electrons and ions. This production of electrons and ions creates a region of ionized flow or plasma around the vehicle. This plasma is known to attenuate the radio frequency (RF) signal from the spacecraft, and transmission is possible only at RF frequencies greater than the characteristic plasma frequency [1]. The plasma frequency is directly related to the electron density around the vehicle, which depends on the vehicle's geometry, flight conditions, and altitude. Communication is restored when the plasma frequencies decrease, which is due primarily to the deceleration of the reentry vehicle to lower velocities. The space shuttle initially experienced a blackout phase of about 16 min and the Mars pathfinder experienced a 30 s radio blackout. The space shuttle used NASA's Tracking and Data Relay Satellite (TDRS) system to communicate through the tail end of the vehicle, where ionization was less to solve the blackout problem [2]. However, the TDRS requires the tail end of the vehicle to have less ionization than the front to maintain communication, and thus cannot be used for ballistic reentry vehicles [3]. During blackout, vehicles cannot receive guidance or maneuvering information from a control center and can travel for hundreds of miles during this loss of communication.

Significantly, for smaller reentry vehicles where the atmospheric destruction is expected to be incomplete or the residual risk for ground population is too high, it is important to notify the ground station of the location of the resulting debris cloud. Consequently, the use of airborne collision-avoidance system (ACAS) technology plays an important role in warning pilots of other vehicles that might pose a threat to collision. This study applies the concept of aerodynamic shaping, which can be used to control the plasma layer to reduce radio blackout, for the design of an alert transmitter [3]. With small, slender geometries, the strength of the resulting shock wave is much weaker; hence, ionization is less, reducing the blackout duration.

The von Kármán Institute for Fluid Dynamics (VKI) is interested in analyzing the blackout phase regarding the design of alert transmitters. An alert transmitter is used to notify ground stations, vessels, and aircraft of the position of reentering objects. To clarify, the reentering object initially hosts the alert transmitter. However, during the object's descent into the atmosphere, destruction will occur between 100 km and 70 km thereby releasing the transmitter and forming a debris cloud as shown in Fig. 1. It is of importance to have an alert transmitter as a payload that will be able to communicate and notify the ground station of the location of the debris cloud. The idea of the transmitter in this study is one option for the reentry vehicle aspect of the reentry direct broadcasting alert system (R-DBAS) by the European Space Agency (ESA) that is intended to provide a more precise location of debris to ground stations [4]. The ESA's concept inspired the research of this study. The R-DBAS is designed to release from its host vehicle when it experiences significant aerodynamic heating, and subsequently determines its own location and computes the final coordinate of the debris footprint that is then broadcast to anyone holding a receiver in the proximity of the hazard area [5]. Most important, the overall mass and drag of the R-DBAS core unit is optimized to achieve a ballistic coefficient that allows direct alert broadcasting coverage of the entire hazard area and of the vicinity [4]. The R-DBAS system will give an airplane about 5–7 min to get out of the way until the debris cloud reaches the flight level; with a typical hazard area being 1000–2000 km long but very narrow (30–70 km), an escape maneuver from the risky area can be readily performed or the aircraft can hold its position until it is safe to cross the hazard area. Therefore, an important aspect in the design of this transmitter is to ensure communication through the blackout phase to extend the warning time to ground stations, thereby providing a more precise location of the debris cloud. Depending on antenna characteristics, the further one starts transmitting will result in a larger coverage area; due to the strong attenuation, an omnidirectional antenna system is not advisable. This study is oriented more toward a general feasibility study for designing the alert transmitter and less on the development of computational models; detailed design considerations, including antenna accommodation and the structural integration of the unit, are yet to be made. The trajectory and heating of the alert transmitter (after the main satellite disintegration) strongly depends on the area-to-mass ratio, which is influenced strongly by the embarked subsystems for communication, which then drive the Electric Power System/batteries, and so forth.

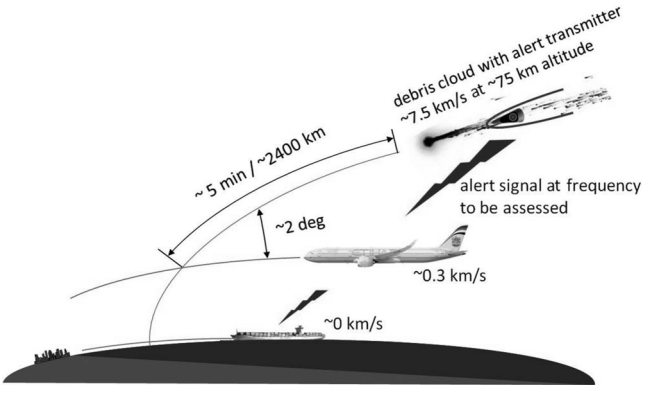

Fig. 1 Alert transmitter communicates the location of the debris cloud to ground stations.

The design of such a device should be undertaken with the main goal of communicating during the blackout phase. In the hypersonic reentry process, a plasma forms around the vehicle that degrades radiowave signal propagation. The plasma frequency is directly related to the magnitude of the electron density, which is related to the vehicle's geometry, freestream velocity, and altitude. Thus, a primary goal of this study is to investigate the flowfields of various geometries at different flight conditions to aid in the design of an alert transmitter. It is known that frequencies above 10 GHz are more subject to atmospheric and rain attenuation. Thus, there is an upper frequency limit in communication during the blackout phase for reentry vehicles.

Equally important, the design of an alert transmitter is an extension of the airborne collision-avoidance system technology already used on aircraft to warn pilots of other vehicles that might pose a threat to collision. Moreover, several events previously occurred that highlighted the importance of increasing the collision-avoidance communication capability for aircraft. For example, Emmanuelli and Sgobba explained in [6] how the uncontrolled reentry of Russia's Phobos-Grunt resulted in the closing of the European airspace for 2 h. Most important, a study conducted by the Federal Aviation Administration following the disintegration of Space Shuttle Columbia in 2003 found that the probability of an impact between Columbia debris and a general aviation aircraft was one in 100 [6]. Furthermore, Emmanuelli and Sgobba explained that predicting the exact location and time of reentry could be difficult due to a skipping effect that debris experienced as they reentered Earth's atmosphere. This effect depended on atmospheric variations of density and winds that were difficult to predict. The trajectory and location of surviving fragments could be precisely predicted only when the "skipping effects" subsided. As a result, the time for the debris to impact the ground or to reach the airspace became short, further illustrating the importance of ACAS technology. According to The Aerospace Corporation, there are about 100 large manmade objects that reenter the Earth's atmosphere uncontrolled each year [6]. Thus, there is a motivation and need for designing improved ACAS technology to mitigate the risk of collision between aircraft and space debris.

Moreover, the ESA's Beagle 2 spacecraft was launched in 2003 on the Mars Express Spacecraft, where communication was lost on the day it was supposed to land on Mars. Due to the failed mission, a board of inquiry was appointed to investigate the failure of the mission and provide recommendations to avoid a similar catastrophe in the future. Out of the recommendations, it was suggested that future planetary missions should have a more robust communication system including a blackout communication capability [7]. The estimated cost of the failed mission included roughly $65 to 80 million U.S. dollars, and thus provided further motivation for mitigating the radio blackout problem. In addition, developing a methodology and approach to analyze the blackout phase for small, slender geometries was relevant, not only to the ACAS concept but also to other currently developed small reentry vehicles. For example, this includes the von Kármán Institute's 3U (10 cm × 10 cm × 30 cm) Cubesat QARMAN (which stands for

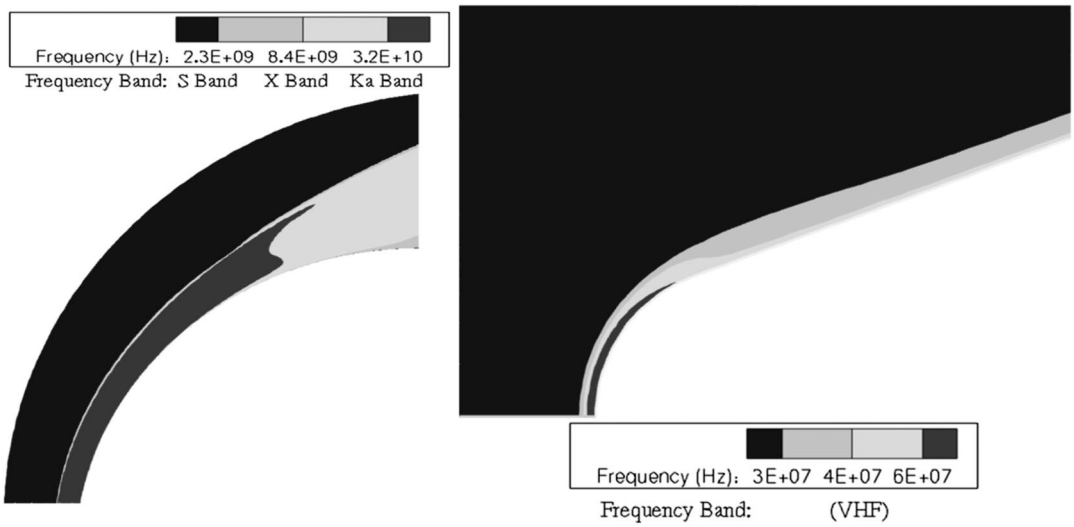

Fig. 2 VHF band already allows communication for the blunt-nosed cone.

QubeSat for aerothermodynamics research and measurements on ablation), which will be launched on the QB50 program. This mission will demonstrate reentry technologies: particularly, novel heatshield materials, new passive aerodynamic drag and attitude stabilization systems, and the transmission of telemetry data during reentry via data relay satellites in low Earth orbit [8]. Likewise, the Orion capsule reentry vehicle is being developed for deep-space manned missions, and future hypersonic high-lift space planes for space tourism or military applications will need to improve their communication capabilities during flight at hypersonic speeds. Thus, estimating when communication will be lost and regained is critical from a guidance, navigation, and control perspective for the design of future space missions and military applications.

Furthermore, large blunt bodies will generate a much stronger shock wave and, as a result, will have a higher electron number density due to the increased ionization, making communication during reentry more difficult. For sharp geometries, Hartunian et al. [2] explained that the boundary layer was laminar at high altitudes and remained thin compared to the RF wavelength, which effectively reduced the attenuation. In addition, for small, slender geometries, the shock wave was much weaker, making communication easier during reentry.

The frequency required to avoid blackout was compared at Mach 26 at an altitude of 80 km for a 1 m radius sphere (left) and a 0.005 m blunt-nosed geometry (right), as shown in Fig. 2. The resulting simulations from the flow solver were postprocessed where the plasma cutoff frequency contour was implemented using Eq. (3). Due to the bluntness effect, ionization levels were high for the sphere, and it was seen that the Ka band (32 GHz) is the only possible frequency that can be used to communicate at an altitude of 80 km. Ka band attenuation is shown in dark gray, and it is the only possible frequency band that can communicate based on the choices displayed. On the contrary, a simulation was computed with the same boundary and freestream conditions for a blunt-nosed cone. The plasma cutoff contour for the blunt cone was found to be significantly lower, allowing for a very high-frequency (VHF) range for communication as opposed to the Ka band for the sphere. Thus, the use of a small, slender geometry would allow for the use of lower-frequency bands at higher altitudes, which are trajectory dependent.

II. Literature Overview and State-of-the-Art Methods for Blackout Analysis

Blackout analyses have been examined by several authors for various reentry missions. The space missions of Project Mercury, Gemini, and Apollo experienced significant minute-long communication blackouts during their reentry [9]. An extensive literature review is done by the present authors to examine current state-of-the-art methodology in predicting and mitigating blackout for reentry vehicles.

In [10], Morabito examined the 30 s blackout of the X-band antenna (8.4 GHz) of the Mars Pathfinder mission. To simulate the Mars reentry, Morabito used two numerical methods, Horton and LAURA, developed by the Jet Propulsion Laboratory and by NASA Langley Research Center. The algorithm used in the Horton program assumed equilibrium conditions; whereas the LAURA program assumed nonequilibrium conditions, which allowed for recombination, thus resulting in a lower electron number density. As a result, the findings from the Horton program were considered conservative in predicting the blackout period. Due to the antenna being mounted in the back shell of the spacecraft to communicate with the Earth, the electron density was calculated in the wake region of the spacecraft. The electron density was assumed to remain constant as it flowed around the spacecraft into the wake region. The approximation did not account for any recombination, and the change in density was due only to the expansion of the gases, and was thus a conservative approach in predicting the blackout period. Morabito used Eq. (1), from [11], to get the ratio of the electron number density in the wake region to the stagnation point:

$$\frac{n_{e/w}}{n_{e/s}} = \left[\frac{\kappa P_{\infty}}{P_G}\right]^{1/\gamma} \tag{1}$$

Most important, Morabito's approach to calculate blackout was based on comparing the electron density to the critical density of the spacecraft's frequency band [10]. The signal would be attenuated for frequencies that fell below the plasma frequency and would be unaffected for frequencies that lay above the critical plasma frequency. More specifically, Morabito used the guideline that, if the electron density lay above the critical density by more than an order of magnitude, then blackout conditions were almost certain. Using this approach, the electron density in the wake region exceeded the critical X-band electron density during the first 20 s of the 30 s blackout period. Morabito explained the difference was likely due to high Doppler dynamics and low signal-to-noise ratio, which may have contributed to the blackout during the last 10 s. This paper focuses on communicating through the back of the spacecraft, and the method described herein can be directly applied to analyze the blackout for reentry vehicles aiming to communicate through the tail end. The methodology used by Morabito in using the plasma frequency and comparing it to a given frequency band is also applied in this study.

Similarly, Reynier and Evans in [12] used the concept of comparing the electron density to the critical electron density of a frequency band to analyze the blackout duration of the inflatable reentry and descent technology flight performed in 2006. The vehicle had an autonomous radio telemetry system (ARTS) operating at a frequency of 219 MHz. Thus, when the critical density of electrons was reached, it was assumed that the communication link was cut.

Two methods were used to calculate the blackout duration. The first method involved using the shock-layer solver PMSSR, accounting for thermal and chemical nonequilibrium to get the chemistry composition along the stagnation line. The electron density was then compared with the critical electron densities at the link frequency. Using this approach, a blackout period of 68 s was found compared to the real blackout duration of 45.3 s. Reynier and Evans explained that the discrepancy (further explained in [13]) might be due to the particular sensitivity to the onset and severity of an electron avalanche phenomenon associated with changes in the thermochemical model. A possibility to improve the first approach was to use electron densities predicted by computational fluid dynamics (CFD) simulations. Subsequently, the second approach by Reynier and Evans [12] involved performing numerical simulations using the CFD solver,TINA, to first find the electron density and then couple the results to a propagation solver. The results from TINA, including the electron mass fraction, electron temperature, and electron number density, were mapped to a three-dimensional (3-D) orthogonal mesh. Maxwell's equations were then used to solve the electric field corresponding to the ARTS transmission through the plasma flow using the electromagnetic solver PLASMA. The coupled approach led to an underestimation of the blackout period. Reynier and Evans proposed that a further study including ablation material effects on ionization could explain the differences between the attenuation predicted and observed.

Regarding the effect of the thermochemical model, Greendyke et al. [13] investigated how the uncertainties of some of the physical models impacted the electron number density profiles calculated for the Aeroassist Flight Experiment. The NASA Langley Research Center's Aerothermodynamic Upwind Relaxation Algorithm (LAURA) was used to obtain numerical solutions for viscous hypersonic flows in chemical and thermal nonequilibrium. A finite rate catalytic wall boundary condition was used, and radiative heat transfer was not used. "Preliminary calculations showed that radiative cooling will lower the vibrational-electronic temperature across the shock, thus reducing the electron-impact ionization rates and lowering the electron number density" [13]. Greendyke et al. also showed that the difference in electron number density was minimal between axisymmetric and 3-D simulations. Significantly, Greendyke et al. illustrated that the choice of chemical rates had a strong influence on the electron number density. The simulations using LAURA revealed a particular sensitivity of the onset and severity of the electron avalanche phenomena due to changes in the thermochemical model. Dunn and Kang's [14] rates provided the largest electron number densities as opposed to rates used by Park in 1987 [15] and 1990 with Gupta's equilibrium constant [16]. It was also explained that the magnitude of the electron density and dual plateau effect were attributed to an electron avalanche effect caused by the onset of electron impact ionization. Greendyke et al. concluded [13] that models that enhanced translational and vibrational-electronic energy exchange in the two-temperature model tended to increase ionization levels in the shock layer.

Furthermore, Hartunian et al. in [2] described possible mitigation schemes to reduce the blackout period for mainly sharp geometries for the purpose of reusable launch vehicles for commercial space applications. Some of the methods described include the injection of quenchants like water, which reduces the overall electron concentration, thus alleviating the blackout period. This was successfully demonstrated on the Gemini 3 reentry capsule where significant levels of signal strength increase during the early portion of water injection were noted by ground stations. Using magnetic windows and the use of building an array antenna capable of forming multiple receiver beams was examined. Another way to mitigate the blackout problem was to use sharp, slender geometries or aerodynamic shaping. For example, one could use a sharp, slender probe containing an antenna to project ahead of the bow shock of a blunt reentry vehicle. For sharp geometries, Hartunian et al. described that the boundary layer was laminar at high altitudes and remained thin compared to the RF wavelength, which effectively reduced the attenuation. Approaches to mitigate the blackout problem were grouped into passive or active approaches, where active approaches were aimed at manipulating the plasma conditions, whereas passive approaches were aimed at the design of the vehicle. Most important, Hartunian et al. stated that aerodynamic shaping was the most practical and influential approach for mitigating blackout. Regarding flight demonstration data, NASA's radio attenuation measurements (RAMs) consisted of seven successful flights, with the principal objective of studying the effects of the reentry plasma sheath upon reentry vehicle communication systems. The mission of RAM A was to determine the effectiveness of aerodynamic shaping and magnetic windows in alleviating the blackout problem, whereas the effectiveness of water added to the reentry plasma flow was successfully demonstrated on the RAM C flight. Furthermore, the RAM C flight was equipped with electrostatic probes to determine the ion density distribution, and the data obtained are currently used by many to validate updated chemistry models. The geometry of all RAM reentry vehicles has been a simple blunted cone. More specifically, the RAM C-I had a nose radius of 15.24 cm followed by a 9 deg half-cone angle. The length of the vehicle was 129.5 cm with a cone base diameter of 61 cm, with a final weight of 121.1 kg [2]. Project RAM resulted in a better understanding of the reentry plasma sheath and blackout alleviation techniques. Many reentry flight experiments performed by NASA and the U.S. Air Force to gain more information about the blackout phenomena were summarized in [9].

The idea of using a small, slender geometry for reentry vehicles was further explored by Savino et al. in [17]. An aerothermochemical model was developed to simulate the reentry ionization chemistry, and it was successfully validated against the RAM C electron density measurements. The model included nine species mixture (O_2, N_2, O, O_2^+, N_2^+, e^-, N, NO, NO^+) where the electron was treated as an additional independent gas species. The numerical software used was Fluent, together with customized functions to implement the corresponding chemistry model. The advantages of using sharp, slender geometries were analyzed, and it was seen that the maximum electron density dropped about four orders of magnitude (10^{10} to 10^6 cm^{-3}) by reducing the nose radius from 0.10 to 0.01 m. Most interestingly, it was confirmed that the plasma wind-tunnel facility at the Department of Aerospace Engineering at the University of Naples could be used for the simulation of communication blackout phenomena because the ionization levels produced were of the same order of magnitude as those encountered during reentry.

Furthermore, Steiger et al. in [18] described that lower electron densities resulted from sharpening the nose radius or moving the antenna to a more aft position. The peak electron density decay equation described in this paper and shown in Eq. (2) illustrates that, by reducing the nose radius by a factor of 2.5, the frequency band will perform above the required performance level for an additional 35,000 kft. Here, $1.5 \leq n \leq 2.5$ and $m = 3$:

$$N_{e_{\text{peak}}} \propto N_{e_o} * \rho_\infty^{1/2} * R_N^m / x^n \tag{2}$$

Steiger et al. [18] also stated that a mass transfer of ablation species into the boundary layer could have a substantial effect on the electron production and a change in the flow characteristics, including temperature, velocity, and boundary-layer thickness. Ablation leads to complex chemistry models, and electron production is due to the alkali impurities in the ablation material. Thus, the effect of ablation on the electron density is modeled by taking into account only the equivalent sodium mass addition [18]. For blunt-nosed reentry vehicles, electron production occurs in the stagnation region with electron density decay along the body. On the contrary, for sharp nose vehicles, viscous dissipation causes the electron density to increase with distance from the apex until an equilibrium value is reached. Most importantly, Steiger et al. describes a recent flight test where high altitude telemetry blackout occurred on a sharp, slender reentry vehicle. The vehicle was a sphere-cone with a 0.63 cm nose radius, 8 deg half-angle, and an X-band circumferential ring antenna placed at the 5 in. station. Plasma attenuation began at 57 km with blackout conditions at 45 km. An analysis indicated that the blackout was due to plasma attenuation, with pattern distortion resulting from a small look angle. Thus, Steiger et al. examined the novel idea of using

aerodynamic shaping along with a real flight test, illustrating that the electron density was reduced by reducing the nose radius.

Furthermore, the effect of angle of attack on the electron density was presented by Lew in [19]. Results were computed for the Air Force Cambridge Research Laboratory (AFCRL) Trailblazer II body at a 12 deg angle of attack. At the windward line of symmetry, there was more than an order of magnitude increase in electron density at 12 deg compared with a 0 deg angle of attack. Most of the increase was due to an increase of the pressure values in the boundary layer at higher angles of attack. Electron density along the windward line of symmetry increased with angle of attack and became nonlinear with larger angles of attack. Thus, reviewing state-of-the-art methods for blackout analysis, it was seen that the innovative idea of using small, slender geometries was a promising approach in reducing the blackout period, and it is further explored in this study.

III. Blackout Phenomenon

A blackout analysis of hypersonic reentry flows involves many various phenomena, as illustrated in Fig. 3, which is reproduced from [20]. The problem involves flows at hypersonic speeds, thermal nonequilibrium, chemical nonequilibrium in the shock layer, gas radiation transfer, and electromagnetic wave damping in the plasma shock layer. When a vehicle flies at hypersonic speeds, a plasma layer is created as a direct consequence of the conversion of the kinetic energy of the vehicle into thermal and internal energy of the surrounding medium via a shock wave [3]. The loss of communication during reentry is caused by the high concentration of free electrons, which are generated around the vehicle. A communication blackout occurs when the electron concentration in the plasma near an antenna reaches or exceeds the critical electron density for a given frequency link or $n_e = n_{\text{cr}}$. For a given electron number density, the plasma frequency in hertz is shown in Eq. (3) [3]:

$$f_p = \frac{1}{2\pi}\sqrt{\frac{e^2 n_e}{\epsilon_0 m_e}} \tag{3}$$

During reentry, temperatures can get exceedingly high, increasing the kinetic energy of the particles. Hence, the number of collisions increases producing free electrons and ions, creating a layer of ionized flow, which can attenuate the radio frequency if the critical electron density for a frequency band is exceeded. The signal will be attenuated for frequencies below the plasma frequency and will be unaffected for frequencies that lie above.

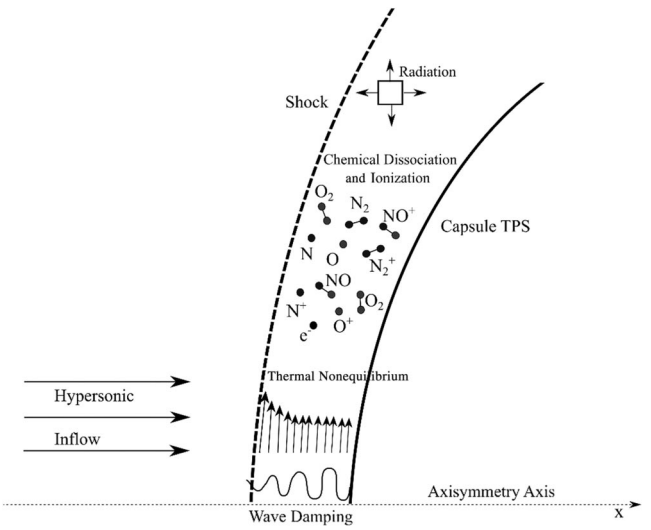

Fig. 3 Illustration of the various shock-layer phenomena associated with the reentry process [20].

A. Nonequilibrium Processes

During hypersonic entry into Earth's atmosphere, a large amount of kinetic energy is converted across a strong shock wave into translational energy of the gas atoms and molecules. For a monatomic gas like helium, this translational kinetic energy is the total energy of the gas. However, for diatomic molecules, there is also energy associated with the rotational and vibrational motions where the total energy of the molecule is the energies associated with translation, rotation, vibration, and electronic excitation [21]. Depending on the shock intensity, different physicochemical processes may take place, such as excitation of the internal energy modes, dissociation of the molecules, and ionization of the atoms and molecules [22]. One can then define a temperature for each mode or a multitemperature model to accurately model the temperature in the postshock region. Computational fluid dynamic simulations of highly nonequilibrium real gases are an area of current research in the design of hypersonic vehicles. A standard approach is to use a two-temperature model where the distributions of energy in the translational-rotational mode are equal ($T_t = T_r$) and the distributions of energy in the vibrational-electronic mode are equal ($T_e = T_v$) [23].

In flow across a shock wave, a fluid element's pressure and temperature are suddenly increased and, as a result, its translational, rotational, vibrational, and chemical properties will change. The fluid element will start to seek new equilibrium properties, but this process requires molecular collisions, which require time. By the time enough collisions have occurred, the fluid element will have moved a certain distance downstream of the shock. Thus, there is a region immediately behind a shock wave where equilibrium conditions do not prevail and a relaxation distance can be defined as the distance downstream of the shock front required for the flow properties to reach 95% of their equilibrium values [24]. In the postshock region in hypersonic flow, the adjustment of translational and rotational modes to changes in the environment requires relatively few collisions; thus, the corresponding readjustment time is short [21]. On the contrary, vibrational and chemical modes are relatively slower to adjust, and thus take more time to come back into equilibrium, as shown in Fig. 4. Hence, chemical nonequilibrium effects will occur because the changes in the chemical composition will take time and reaction rates will be needed to describe the change in composition of a given species.

In this study, thermal equilibrium and chemical nonequilibrium are assumed; thus, one temperature is used to describe the temperature of the various energy modes of the molecules. To model chemical nonequilibrium effects, a reaction file with the necessary rate constants is implemented into the numerical solver. Modeling a shock layer with the assumption of thermal equilibrium effectively means to reduce the relaxation zone to zero size. Therefore, the modeling under such an assumption results in a higher amount of electrons in the vicinity of the shock, and is thus conservative with respect to the blackout prediction. As the current study addresses a design assessment of the alert transmitter, the authors considered this a suitable approach.

B. Propagation of Electromagnetic Waves in a Plasma

The propagation of electromagnetic waves is governed by Maxwell's equations, and the following discussion is for a uniform, unbounded, and nonmoving plasma, as described by Mitchner and Kruger in [25]. Taking the time derivative of the Maxwell–Ampere equation, the electric field can be expressed as Eq. in (4):

$$\nabla^2 E - \mu_0 \epsilon_0 \frac{\partial^2 E}{\partial t^2} = 0 \tag{4}$$

The general form of the transverse wave solution of Eq. (4) in the x direction can be modeled as a complex amplitude, E_0 multiplied by a complex phase factor:

$$E(x,t) = E_0 e^{ikx - i\omega t} \tag{5}$$

where x is the three-dimensional position in space, k is the wave number that may be complex, and ω is the angular frequency of the wave. If one assumes that the plasma consists of an equal number of

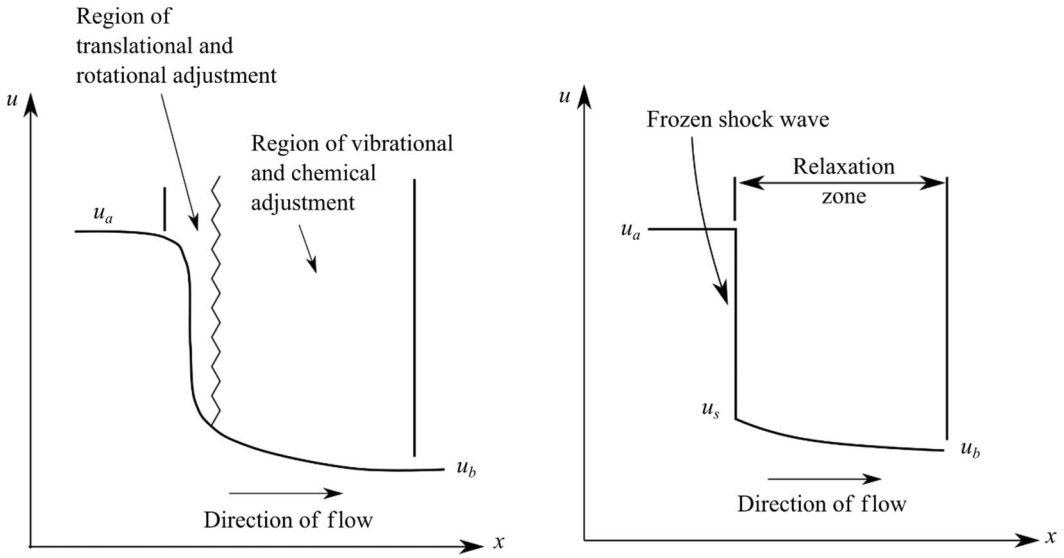

Fig. 4 Illustration that the adjustment time for the translational and rotational modes is much faster than the vibrational and chemical adjustment time [21].

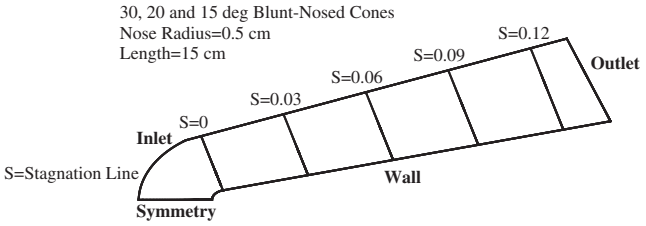

Fig. 5 During postprocessing, the electron density is examined at various increments along the wall.

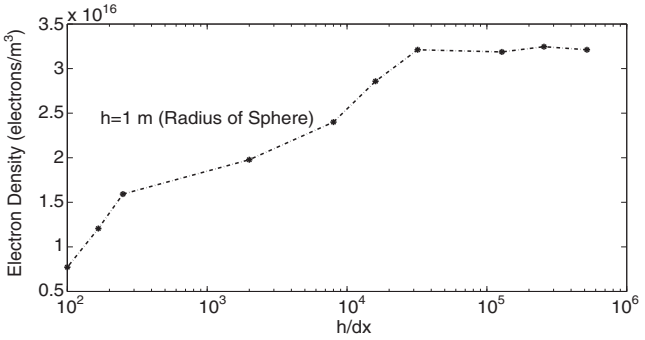

Fig. 6 As the mesh is refined at the wall, the electron density converges.

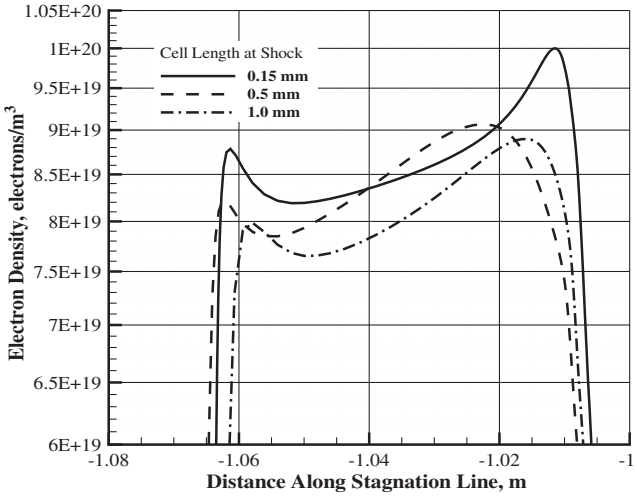

Fig. 7 Effect of refining shock leading to an increase in the electron density at the body where the sphere is located at $x = -1$.

positive ions, free electrons, and neutral particles, the charged particles maintain an average equilibrium distance as a result of electrostatic forces. Any displaced charge will oscillate about its equilibrium position, where the frequency of oscillation of the charged particle is called the plasma frequency, as described in Eq. (6):

$$\omega_p = \sqrt{\frac{e^2 n_e}{\epsilon_0 m_e}} \tag{6}$$

More important, in an ionized gas, the permittivity is frequency dependent and generally becomes low, depending on the plasma frequency ω_p and angular frequency ω, and can be expressed as in Eq. (7), as described by Takahashi et al. [26]:

$$\varepsilon(\omega) = \varepsilon_0\left(1 - \frac{\omega_p^2}{\omega^2 + \upsilon_e^2}\right) \tag{7}$$

Electromagnetic waves cannot travel into a medium if $\omega_p^2 > \omega^2 + \upsilon_e^2$ because the permittivity will be negative, resulting in an imaginary refraction index, implying that the electromagnetic wave is reflected from the surface or becomes an evanescent wave. In other words, when the electromagnetic wave passes through a region where the electron density exceeds the critical value for the link frequency attenuation, refraction or reflection can occur. Being that the plasma frequency is greater than the link frequency, the charges in the plasma have sufficient time to shield its interior from the electromagnetic field.

C. Blackout Computation Method

In determining if blackout conditions will occur, the plasma cutoff frequency equation from [3] [Eq. (3)] is used. If the plasma frequency is greater than a given frequency band, then the signal will be interrupted. For each given frequency band, Eq. (3) can also be used to find the critical electron density associated with it, as shown in Eq. (8). Refer to [3] for the critical electron densities for various frequency bands with their applications:

$$n_{e_{\text{cr}}} = \frac{f_{\text{link}}^2}{80.64} \tag{8}$$

Using this approach, to state whether blackout conditions will occur for a given frequency band, the methodology from Morabito

Table 1 Freestream conditions *C*1

Symbol	Quantity	Value
M	Mach number	26.5
Z	Altitude	80 km
V	Velocity	7500 m/s
A	Angle of attack	0 deg
T	Temperature	198.6 K
p_∞	Pressure	1.052 Pa

[10] is used. Therefore, if the electron density lies above the critical electron density by more than an order of magnitude, blackout is likely. If the electron density lies below the critical electron d ensity by more than an order of magnitude, blackout is unlikely. Finally, if the calculated electron density is within an order of magnitude of the critical electron density, blackout is uncertain but possible [10].

This methodology for predicting blackout was used in [10,12,17]. For this study, hypersonic simulations are first conducted in the commercial software CFD + +, where Dunn and Kang's reaction file from [14] was used to model the flow chemistry. Due to the high speeds, an ionized flow would become present around the vehicle, which was then postprocessed. The plasma critical density for a frequency band was plotted against the electron density at various locations along the geometry, which was also extensively used in literature, including by Savino et al. [17]. If the electron density was more than an order of magnitude greater than the critical density, blackout conditions were assumed.

Subsequently, it was well established that gas-phase radiation was important for the thermodynamic modeling of high-temperature gases for much higher reentry speeds than the considered 7.5 km/s relevant for the low-Earth-orbit return mission examined in this study. Therefore, it was not modeled here. For this study, the authors followed the rationale of [3,10,11], where it was consistently argued that the electron neutral collisions did not substantially alter the attenuation of the wave propagation. The minor contributions of the thermodynamic effect were considered beyond the scope of this research.

D. Implementation of Software

ANSYS ICEM CFD is used for mesh generation and CFD++, which incorporates a finite volume framework and is used as the numerical solver to perform hypersonic CFD simulations. The electron density is then postprocessed to determine if communication is possible and at what frequency band. The commercial code CFD++ by Metacomp Technologies was developed for high-speed applications and was extensively validated for supersonic and hypersonic flow regimes [27]. In addition, an arbitrary number of species and chemical kinetics can be implemented into the solver, which are solved in close coupling with the fluid dynamic equations, allowing the equations to be advanced at a rate determined by the fluid dynamics and not by the underlying kinetics [23].

1. Numerical Methods

A compressible real-gas Navier–Stokes with viscous terms is used for all simulations, together with Dunn and Kang's reaction file from [24], to simulate the chemical nonequilibrium effects of the flowfield. The governing equations that are being solved by the solver include Eqs. (9–13) and are taken from [24]:

Global continuity:

$$\frac{\partial \rho}{\partial t} + \nabla \cdot (\rho \boldsymbol{V}) = 0 \tag{9}$$

Species continuity:

$$\rho \frac{\mathrm{D}c_i}{\mathrm{D}t} + \nabla \cdot (\rho_i \boldsymbol{V}_l) = \dot{w}_l \tag{10}$$

x momentum:

$$\rho \frac{\mathrm{D}u}{\mathrm{D}t} = -\frac{\partial p}{\partial x} + \frac{\partial \tau_{xx}}{\partial x} + \frac{\partial \tau_{yx}}{\partial x} \tag{11}$$

y momentum:

$$\rho \frac{\mathrm{D}v}{\mathrm{D}t} = -\frac{\partial p}{\partial y} + \frac{\partial \tau_{xy}}{\partial y} + \frac{\partial \tau_{yy}}{\partial y} \tag{12}$$

Energy:

$$\rho \frac{\mathrm{D}h}{\mathrm{D}t} = -\nabla \cdot \boldsymbol{q} + \frac{\mathrm{D}p}{\mathrm{D}t} + \Phi \tag{13}$$

where Φ is the dissipation function given by

$$\Phi = \tau_{xx}\frac{\partial u}{\partial x} + \tau_{yy}\frac{\partial v}{\partial y} + \tau_{xy}\left(\frac{\partial u}{\partial y} + \frac{\partial v}{\partial x}\right) \tag{14}$$

The reaction file assumes that air is composed of 11 species, including O_2, N_2, O, O_2^+, N_2^+, e^-, N, NO, NO^+, O^+, and N^+. The effects of different thermochemistry models on the electron density are outside the scope of the present work and will be considered for future work. Since the given problem involves high temperatures, a five-temperature range is used to find the thermodynamic properties of the specific heat, enthalpy, and Gibbs free energy of a given species.

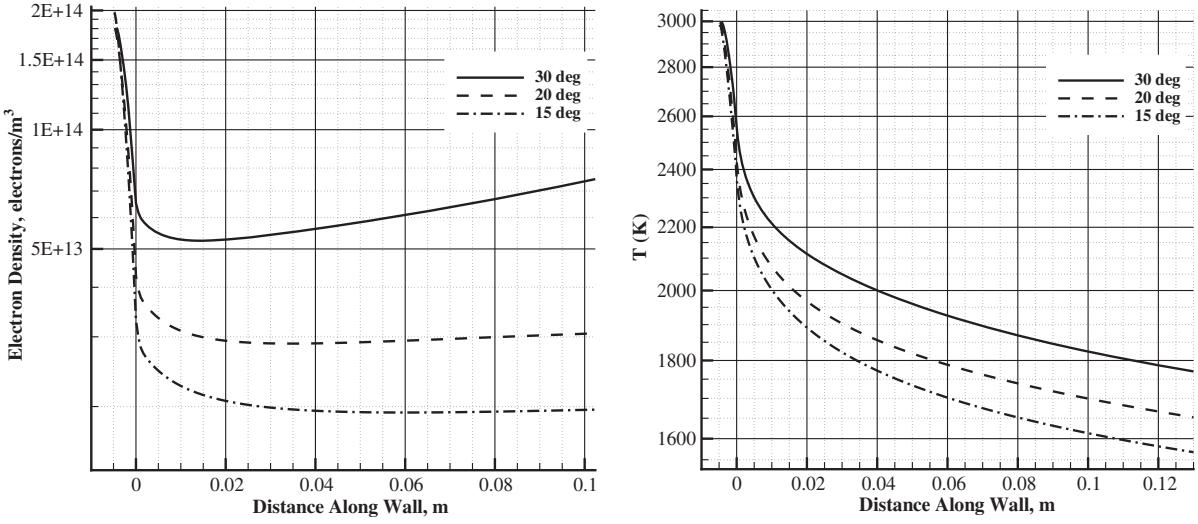

Fig. 8 The 30 deg cone has increased ionization and a higher temperature along the wall.

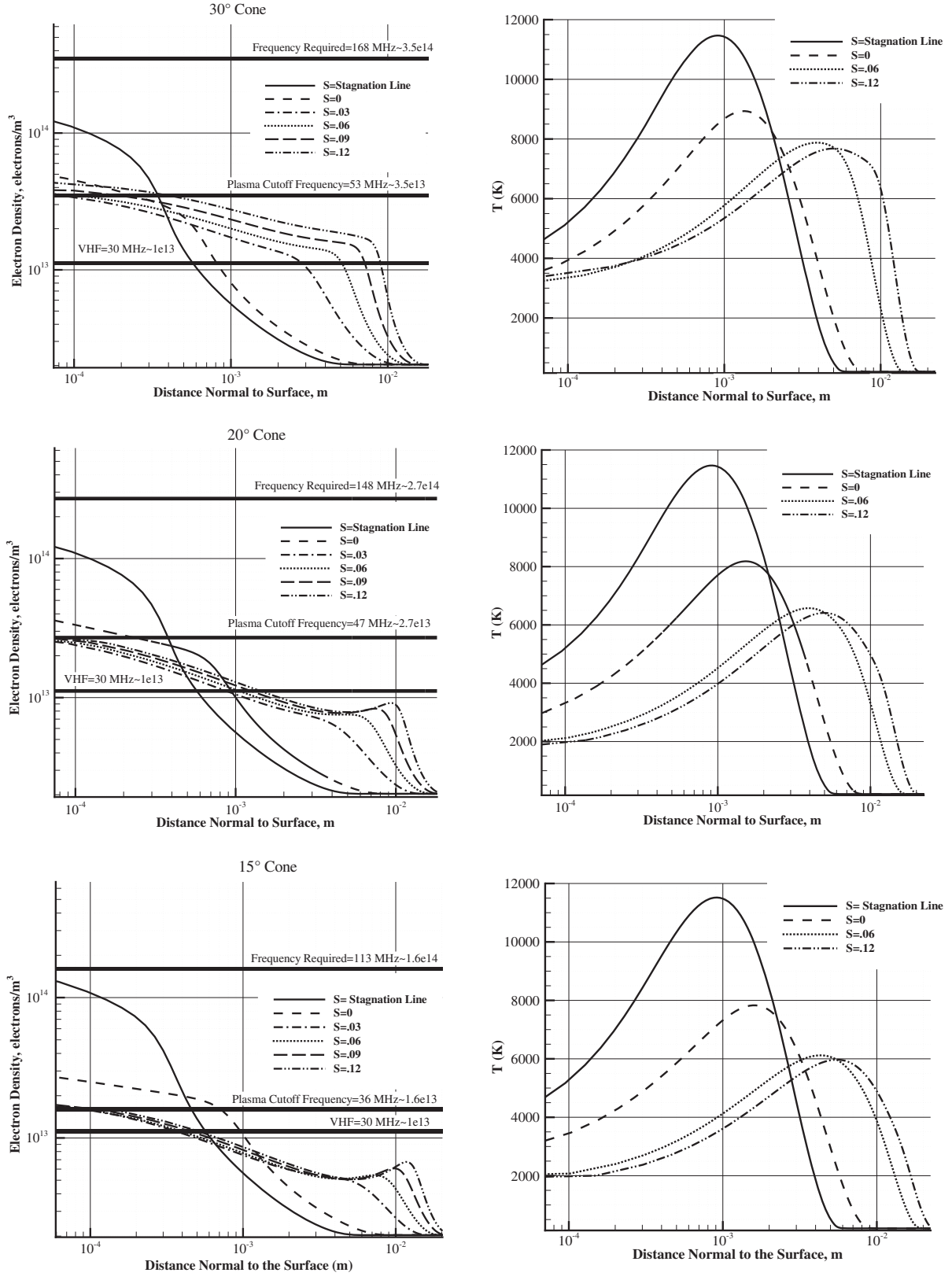

Fig. 9 Electron density and temperature profiles for various slice locations.

A Reynolds-averaged Navier–Stokes model with no turbulence is used to simulate a laminar flow. The carbuncle control switch is activated, which is used when fine grids are simulated at high Mach numbers. The carbuncle phenomena can show up as a recirculation bubble near the nose of the geometry at high freestream velocities. Activating this control avoids the carbuncle phenomena by adding dissipation to the shear layer where the additional dissipation is localized to sensitive regions based on the pressure ratio. Simulations are computed at a two-dimensional (2-D) axisymmetric boundary condition including a steady-state formulation with an implicit scheme. The spatial

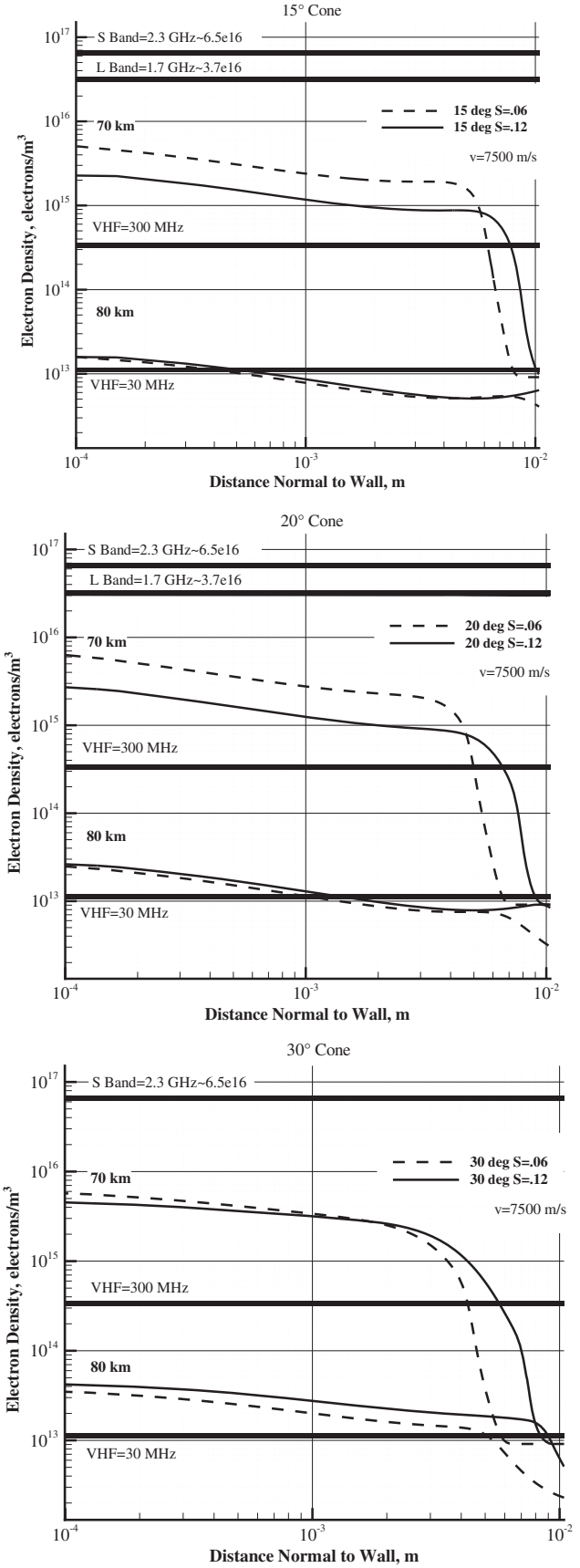

Fig. 10 Electron number density profiles at 70 and 80 km for two antenna locations.

discretization involves blending between the first and second orders. The pressure and temperature at various altitudes are evaluated using the 1976 U.S. Standard Atmosphere model from [28].

2. Boundary Conditions

Radiative heat transfer is used at the wall where the user-supplied temperature at infinity is set equal to the freestream temperature. The wall heat flux is then computed using Eq. (15), as described in [29]:

$$\epsilon\sigma(T_b^4 - T_\infty^4) = k\frac{\mathrm{d}T}{\mathrm{d}n} \tag{15}$$

An emissivity of 0.85 is used with the wall temperature relaxation feature that is usually needed for high-Mach-number flows. The radiative heat transfer boundary condition is used with a noncatalytic wall condition. In the reentry process, atomic species can recombine in the boundary layer and at the vehicle surface, thus releasing the reaction energy and increasing the thermal load [30]. If the material at the surface does not promote atomic recombination, then it is described as a noncatalytic wall. In a supercatalytic condition, the concentrations of the species that exist in the freestream are assumed at the wall. The wall then acts as a supercatalyst to all species and not only turns ions into neutrals but also recombines all atoms and molecules to reproduce a specific state of species at the wall [29]. This formulation, which is used in the commercial CFD software package CFD++, can overpredict recombination rates and temperatures. Due to this fact and the relatively low relevance of the surface chemistry model, all simulations incorporate a noncatalytic wall condition. Only a supercatalytic condition is used to perform the grid independence study, which is based on a computational case provided in the CFD++ *User Manual*. The computational case is initially used to verify the correct use of the commercial code. To model the hypersonic flow at the inlet, the supersonic inflow boundary condition is used, with the outlet condition being centroidal extrapolation, assuming the flow is exclusively supersonic outflow, as shown in Fig. 5. A symmetry boundary condition is used along the x axis to model the 2-D axisymmetric hypersonic flow.

3. Postprocessing

After simulations were performed with CFD++, the flow data were postprocessed. Analyzing the blackout period, it was needed to see the variation of the electron density normal to the surface. This was because the electron density could have been highest at the wall or some distance away. As a result, lines were made perpendicular to the surface to extract the values of the electron number density at various locations away from the tangency point (or where the sphere meets the cone) for different cone angles, as shown in Fig. 5. The parameter S was defined in meters, and its frame of reference was along the wall of the blunt-nosed cone geometry. Postprocessing was also used to determine the location of the shock wave before a grid adaption was performed in ANSYS ICEM CFD.

IV. Grid Independence Study

A grid independence study was first performed where the effect of mesh refinement on the electron density at the stagnation point was examined. Significantly, the method of using the electron density obtained from CFD simulations to predict the blackout phase implied that it was exceedingly important to have a mesh that captured the electron density accurately. The method and approach to this grid independence study were taken from the work of Quanhua et al. in [31]. The simulations for this study were conducted for the hypersonic flow over a sphere, where the cell at the shock wave and at the wall was refined. Analyzing Fig. 6, it was seen that the electron density at the stagnation point began to converge as the cell size was reduced at the wall and eventually became mesh independent. As a note, dx is defined as the cell length, which is normalized by the radius of the sphere h. After performing this grid independence study, the cell length required to capture the electron density accurately at the wall was also used in refining the shock wave.

Since the bluntness or blockage was larger for the 1 m sphere compared to the smaller cross-section cone geometry considered for the alert transmitter, a finer mesh was done on the cone geometry to check that the mesh was sufficient in resolving the flowfield. A justification of the validity of the conclusions extracted from a

sphere to the simulated domain was that the simulations for the blunt-nosed cone were in good comparison with the flight-test results reported in [18], which are discussed later in the paper. Accordingly, after finding the mesh independent size at the wall, the effect of refining the shock region on the electron density was examined. The previous mesh independent value found was used at the wall, whereas the cell length at the shock was altered. It was observed that, as the cell size was refined at the shock location, there was an increase in electron density at the body, as shown in Fig. 7. Therefore, refining the shock location was important if one desired to have an accurate prediction of the electron density, and hence to predict the blackout duration. As a result, all blackout simulations included mesh refinement at the wall and at the shock location.

V. Blackout Prediction Results

The primary purpose of this paper is to analyze the blackout phase for designing an alert transmitter, which is used to notify aircraft of possible collisions during the reentry process. This concept is in the beginning stage of development, and this research hopes to serve as motivation for showing that this idea is feasible from a communication perspective. Reviewing the state-of-the-art methods for blackout analysis, it is seen that aerodynamic shaping is a promising approach in mitigating the blackout period. Furthermore, [17] demonstrated that the maximum electron density dropped about four orders of magnitude (10^{10} to 10^{6} cm^{-3}) by reducing the nose radius from 0.10 to 0.01 m. Thus, the chosen geometry to be simulated included a blunt-nosed cone with a nose radius of 0.005 m and a length of 0.15 m, with the initial freestream conditions of Table 1. The length of 0.15 m was a first design estimate that was based on using the CubeSat standard as the underlying bus/satellite for flight qualification of the alert transmitter. The length further depended on the selected cone angle and on the subsystem/batteries used, and it should be small enough to keep the impact on increasing the volume/mass of the satellite small. The CubeSat mission would be an in-flight testing, and the transmitter would embark on larger satellites undergoing an uncontrolled reentry at end of life. The freestream conditions in Table 1 represent the freestream conditions when a spacecraft reenters from a low-Earth-orbit mission [17]. Also, the shape/mass of the parent vehicle is unknown; therefore, to be conservative, a higher velocity was assumed with no strong deceleration at high altitudes.

The different cone angles investigated include 15, 20, and 30 deg. The electron number density depends on the vehicle's geometry, freestream conditions, and altitude; thus, the engineering approach for this study involves conducting numerical simulations at different cone angles, different freestream conditions, and finally different altitudes. In determining if there is a blackout condition or not, the electron density is compared to the critical electron density for different frequency bands. More specifically, a primary goal is to find the location of an antenna with the corresponding frequency band that will allow communication during the reentry process for the alert transmitter.

From a communication standpoint, it might be best to communicate directly in front of the vehicle as opposed to a more aft position perpendicular to the surface. As a result, communications perpendicular to the surface and along the stagnation line are both examined. This method is accomplished by extracting perpendicular slices during postprocessing along the stagnation line and at various increments along the wall of the cone, as shown in Fig. 5. As a result, it is possible to pick a location for an antenna and compare the effectiveness of communicating directly in front of the vehicle or perpendicular to it. As a note, the antenna is not surface mounted but embedded or behind the thermal protection system (TPS), which requires RF transparent TPS material.

A. Cone Angle Effect

The first parameter examined for the blunt-nosed cone was the effect of different cone angles on the electron density. The mesh was refined at the shock position and after the simulation; the electron density contours were extracted at various positions. These simulations were computed with the C1 freestream conditions described in Table 1. Initial simulations involving the blunt-nosed cone resulted in seeing no electrons in the flowfield, which was believed to occur because the numerical method did not work well if no negligible amount of electrons were modeled in the freestream. To alleviate this problem, a small mass fraction of electrons (1×10^{-13}) was seeded into the freestream boundary conditions. A lower level was not possible due to a lower limit of initializing the species mass fraction in CFD++. Similarly, Reynier and Evans in [12] performed their blackout simulations with a very low mass fraction of electrons: 10^{-20}. Reynier and Evans stated that, if a very low mass fraction was not used at the inflow, it might result in an overestimation of the electron density in the whole field.

It is illustrated in the left of Fig. 8 that the 30 deg cone has the highest ionization levels. This is attributed to the increased bluntness, and hence stronger shock wave, for the 30 deg cone. The ionization level for all three investigated cases is high at the front, subsequently decreases downstream of the flow, and then increases again toward the end of the vehicle. The latter effect is pronounced for the 30 deg cone and only small for the other smaller cone angles. This effect, which may be first perplexing, can be explained by two-dimensional flow dynamics. For example, the region, which is very hot and ionized, is very small close to the stagnation point. However, downstream, this region becomes larger, less compressed, and cooler,

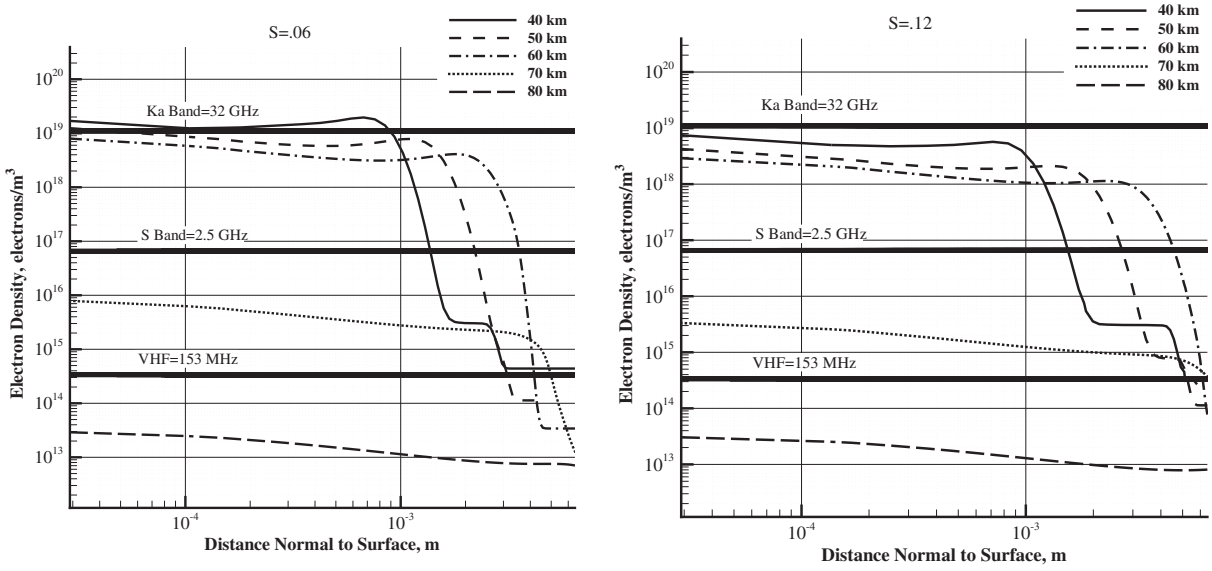

Fig. 11 Frequency band requirements for various altitudes for the 20 deg cone at two antenna locations.

Table 2 frequency band requirements for various altitudes for the 20 deg cone

Altitude, km	Frequency required, GHz	Antenna location, m
80	0.153	$S = 0.06$ or $S = 0.12$
70	2.5	$S = 0.06$ or $S = 0.12$
60	32	$S = 0.12$
50	32	$S = 0.12$
40	Blackout conditions	Blackout conditions

as can be seen on the right of Fig. 8. Nevertheless, the region remains hot enough to sustain or promote ionization. Due to the overall low ionization levels and the less emphasized increase in the downstream direction, the 15 deg cone seems to be the best configuration in alleviating the blackout problem.

As evidence, the temperature distribution along the wall in Fig. 8 depicts the highest temperature for the 30 deg cone, supporting the fact that there is increased ionization. The temperature at the stagnation point is equal for all three cone angles because the nose radius of 0.005 m is the same for all three cases. From a design and manufacturing perspective, the upper temperature limit that ceramic materials can withstand is ~2000 K. However, 30 deg exceeds the ceramic material temperature limit at an estimated distance of $S < 0.04$ m, as shown in Fig. 8. Ablative materials can then be used in the front of the vehicle ($S < 0.04$ m), subsequently followed by ceramic materials. However, ablative materials can occupy space in the nose region of the vehicle and, as a result, the best placement for an antenna is estimated to be at the interface between ablative and nonablative materials, or at a location of $S > 0.06$ m. To clarify, these drawn conclusions on the material choice are valid for the sole conditions simulated. In addition, the material choice also depends on the transparency of the material to RF waves in addition to the maximum temperature limitations. The selection of the thermal protection system material for the alert transmitter is not made yet; therefore, ablation products are unknown. The effect of ablation on the blackout duration is outside the scope of the present work and will be examined in future studies. However, regarding the effect of the ionization levels due to ablation materials such as carbon composites, Farbar et al. [32] examined the effects of ablation on ionization levels for the Stardust spacecraft, which used a phenolic-impregnated carbon ablator. Farbar et al. found that the concentration of electrons and ions along the stagnation streamline was larger for the simulation that did not include ablation, explaining that energy that may be used to ionize particles was instead used in reactions with ablative species

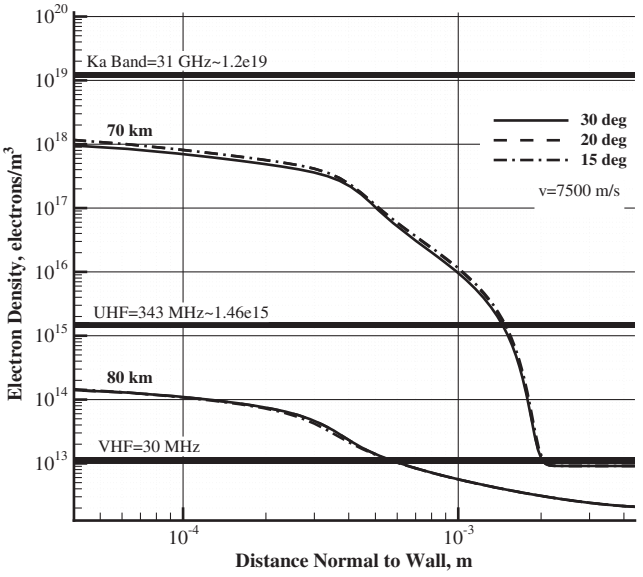

Fig. 12 Communication along the stagnation line is independent of cone angle.

when ablation was included. Along the wake symmetry line, the predicted ion and electron densities with and without ablation were similar.

Analyzing the effect of the cone angle on the electron density, different slices were taken along the surface of the cone, including the stagnation line. Using Eq. (8), the critical density for a given frequency band was plotted against the electron density at different locations. The plasma cutoff frequency shown in Fig. 9 was calculated by assuming the antenna was to be located perpendicular to the surface at a distance of $S = 0.06$ m or $S = 0.20$ ft along the wall of the cone. It was seen that, as the cone angle decreased, the required frequency band for communication decreased. Most important, when choosing the antenna location at $S = 0.06$ m, all three cones could communicate effectively with a VHF band down to 80 km, assuming a velocity of 7.5 km/s. In addition, the temperature slice profile also seen in Fig. 9 illustrates that the temperature at the back of the 30 deg cone was highest and subsequently decreased as the cone angle decreased, conveying that increased bluntness led to larger ionization regions. The surface temperature at $S = 0.12$ m was seen to be slightly greater than that at $S = 0.06$ m for the 30 deg cone in Fig. 9, which the authors believe should not be the case. A possible reason is that the simulation did not reach a steady-state condition.

B. Altitude Effects

Numerical simulations were then performed at two different altitudes (70 and 80 km) to analyze the effect on the electron density and to find what frequency band would be required to avoid blackout conditions. As previously stated, since the shape/mass of the parent vehicle was unknown, to be conservative, a higher velocity was assumed with no strong deceleration at high altitudes. Examining Fig. 10, for an antenna location at $S = 0.06$ m, the VHF at 300 MHz was sufficient to avoid blackout conditions for all three cones at an altitude of 80 km. However, to avoid blackout conditions at 70 km, an S-band frequency range (2.3 GHz) had to be used. Furthermore, as illustrated in Fig. 10, moving the antenna location from $S = 0.06$ to 0.12 m would allow for the use of a lower-frequency range to avoid blackout conditions or for a shift from an S- to an L-band frequency range for the 15 and 20 deg cones.

With the design of the alert transmitter, it will be beneficial to ensure communication to the ground station at even lower altitudes than 80 km. The intermediate cone angle of 20 deg is then simulated at lower altitudes with a fixed velocity of 7.5 km/s. Depending on the flight-path angle and the ballistic coefficient, the speed of the reentry vehicle will be smaller but of the same order of magnitude, therefore assuming the same speed of 7.5 km/s down to 40 km is conservative and enables accurate understanding of physics. Figure 11 displays the frequencies that must be used to maintain communication for the 20 deg cone at various altitudes for two antenna locations of $S = 0.06$ and 0.12 m. Due to the increased pressure and temperature, and hence ionization levels at lower altitudes, it is seen that communication starts to become difficult at 60 km. Communication becomes possible at altitudes of 60 km or lower with an antenna placement at $S = 0.12$ m using the Ka frequency range. At 40 km, it is seen that the electron density starts to equal the critical electron density for the Ka band. Thus, blackout conditions are highly likely beginning at 40 km. These results are summarized in Table 2.

Communicating along the stagnation line might be preferred; thus, this option was also examined. It was found that communication along the stagnation line was more difficult due to the peak aerodynamic heating, resulting in a higher electron density at the nose of the cone. Communication along the stagnation line was possible with an ultrahigh frequency (UHF) band down to 80 km, and subsequently requires a Ka band down to 70 km to avoid blackout conditions, as illustrated in Fig. 12. Using the Ka band as the upper frequency limit, it was seen that blackout conditions would be likely at altitudes lower than 70 km for communication along the stagnation line. Most important, communication along the stagnation line is independent of cone angle.

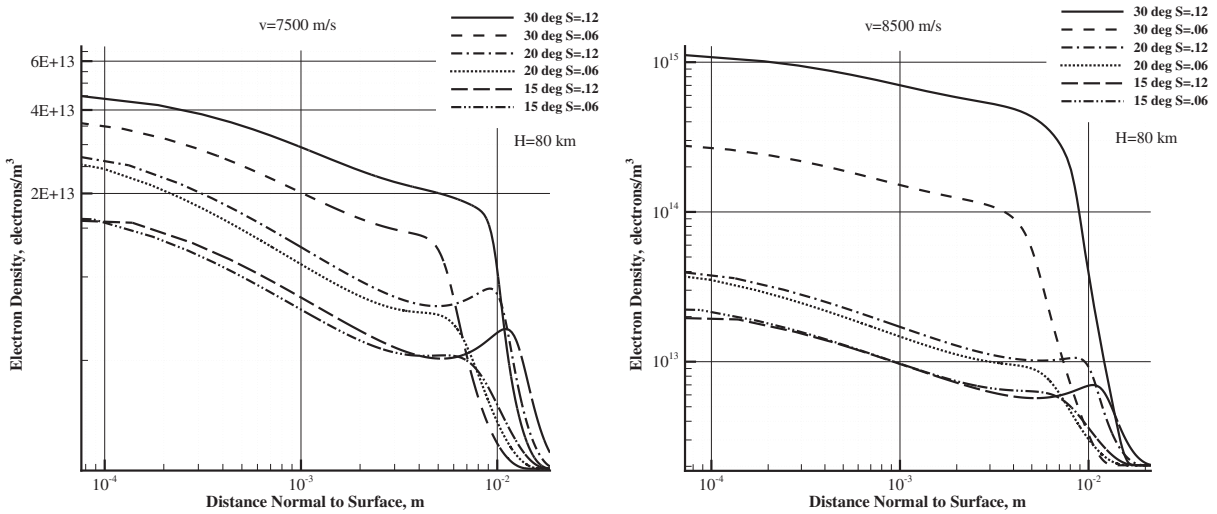

Fig. 13 Decreasing the cone angle results in a shifting of the reaction zone downstream.

C. Freestream Effects

The effects of altering the freestream conditions on the electron density were also examined. One simulation was conducted at Mach 26 and another at Mach 30. It was seen that, as the cone angle decreased, there was a shifting of the reaction zone further downstream, as shown in Fig. 13. In addition, increased bluntness led to larger ionization regions. For example, for the 30 deg cone, there was more ionization in the aft region, and thus the antenna placement should have been forward $\sim S = 0.06$ m. This became even more pronounced at a freestream condition of Mach 30. However, for the 15 deg cone at the Mach 26 case shown in the following, one can see how the placement of the antenna does not depend on freestream conditions as opposed to the 30 deg cone. Thus, as the cone angle decreased, there was a shifting of the reaction zone downstream. Due to the shifting of the reaction zone for smaller cone angles, higher Mach numbers were seen to have less of an impact on determining the location of the antenna. As the cone angle decreased to 15 deg, placement of an antenna in the aft position as opposed to the front was not as critical as compared to the 30 deg cone. Thus, in Fig. 13, one can see how higher Mach numbers led to higher ionization regions for increased bluntness.

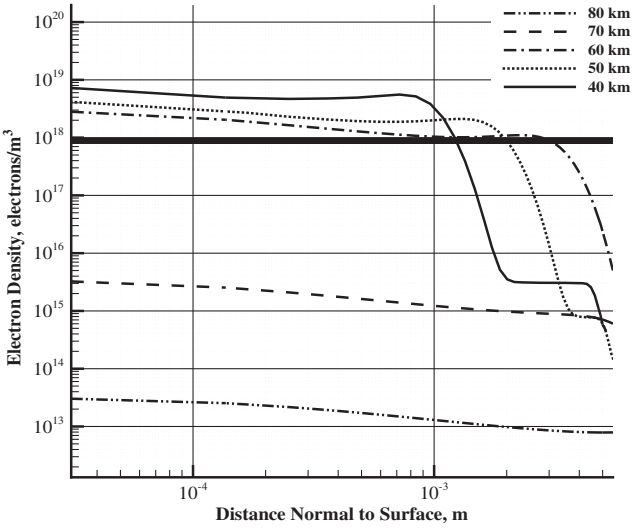

Fig. 14 Computational results illustrating that plasma attenuation begins ~60 km to blackout conditions at ~40 km, thereby demonstrating good comparison with literature.

D. Crosscheck with Literature Results

The blackout computation method used in this study for the application of sharp, slender geometries was then compared with results reported in the literature. Steiger et al. [18] reported blackout was experienced on a sharp, slender vehicle having a 0.63 cm nose radius and an 8 deg half-angle with an X-band antenna at the 5 in. station. Plasma attenuation began at 57 km with blackout conditions at 45 km. To compare the CFD results in predicting the onset of blackout, a slice was made at the 5 in. station ($\sim S = 0.12$ m) for the 20 deg cone at various altitudes. Figure 13 illustrates that, as the cone angle decreased, there was a shifting of the reaction zone downstream; as a result, there was not much difference in the ionization level for the 20 and 15 deg cones at the $S = 0.12$ m point. Thus, it was inferred that the comparison of the 20 deg cone simulation with the actual 8 deg cone geometry would be analogous to crosscheck the blackout computation approach. Examining Fig. 14, the critical electron density for the X band was plotted with the corresponding electron density for various altitudes. It was noted that, at 60 km, the electron density for the 20 deg cone started to exceed the critical density for the X band, and thus plasma attenuation began. At 40 km, the electron density began to be an order of magnitude greater than the critical density, thus ensuring blackout conditions. Therefore, the CFD simulations were in good comparison in predicting the onset of blackout, as reported in [18].

VI. Conclusions

The tradeoff of different cone angles, antenna locations, and the possibility of communicating along the stagnation line or at the aft of the vehicle is investigated at different flight conditions for the design of an alert transmitter. Conclusions from the study illustrate that small blunted cones experience less radio blackout due to the decreased ionization regions encountered as a result of a weaker shock wave. As a result, the 15 deg cone is seen to be best in terms of communicating through the blackout period. Equally important is that, as the cone angle decreases, an increase in electron density occurs further downstream due to a shifting of the reaction zone. As a result, higher Mach numbers are seen to have a smaller impact on the location of the antenna due to a shifting of the reaction zone. In addition, communications along the stagnation line and perpendicular to the vehicle are both investigated. Communicating normal to the wall at a distance of $S = 0.12$ m allows the vehicle to communicate with a very high-frequency band down to 80 km, and it requires an L band down to 70 km. Communication through the blackout phase at altitudes down to 60 and 50 km can be achieved using a Ka band, with blackout conditions becoming likely down to 40 km. Significantly, communication along the stagnation line is independent of the cone

angle and is possible with a ultrahigh frequency band down to 80 km, and subsequently requires a Ka band down to 70 km. However, blackout conditions are likely for altitudes below 70 km. The blackout computation method used in this study is then validated with results reported in the literature. The results prove that the design of an alert transmitter is feasible from a communication perspective.

This research can provide insight to new technologies, including the reentry direct broadcasting alert system by the European Space Agency, which is intended to provide more precise locations of debris to ground stations. The results from this study also expand the available database for comparison hypersonic experiments and simulations, and they may inform future designers in making important design decisions in hypersonic applications including vehicle geometry or antenna location selection.

However, this is only a feasibility study examining the communication aspect during the blackout phase and is a prelude to a more detailed design project where other tradeoff studies will be performed. For example, one of the major tradeoffs in going to a slender geometry is nose heating vs ionization, which will be addressed in future work. During postprocessing, the procedure for predicting blackout conditions is comparing the critical electron number density with the simulated electron number density. Thus, if the electron density is above the critical electron density for a given frequency band, blackout is deemed likely, as discussed in [10], which allows for some margin in the blackout prediction. In addition, modeling a shock layer with the assumption of thermal equilibrium is conservative with respect to the prediction of the electron density, and hence blackout prediction. Likewise, there is also some uncertainty in the blackout computation method because only one reaction set is used. To improve accuracy of the computational fluid dynamics simulations, future work will involve examining how the electron density is affected by including the use of different thermochemical models. Furthermore, future work will consider how the ionization is affected by ablation and the use of a multitemperature model.

Acknowledgments

The authors would like to first thank several people for making this opportunity financially possible. The authors would like to thank the Department Chair of the University of Florida's Mechanical and Aerospace Engineering Department, David Hahn, for awarding the Knox T. Milsaps Memorial Scholarship and making this opportunity possible. Likewise, the authors would like to express thanks to Therese Moretto from the National Science Foundation (NSF) for awarding an NSF research grant to make the internship opportunity possible at the von Kármán Institute for Fluid Dynamics (VKI). The authors would also like to express thanks to Anne Donnelly and the University of Florida's University Scholar's Program for their support. The authors would also like to thank Aaron Ridley, Cheri Johnson, and Eidilia Thomas from the University of Michigan for all of their help and support. Most important, the authors would like to thank the VKI and Jean Muylaert, the Director of the VKI, for accepting Sahadeo Ramjatan's application for this short training program.

References

[1] Kim, M., Keidar, M., and Boyd, I. D., "Analysis of an Electromagnetic Mitigation Scheme for Reentry Telemetry Through Plasma," *Journal of Spacecraft and Rockets*, Vol. 45, No. 6, 2008, pp. 1223–1229. doi:10.2514/1.37395

[2] Hartunian, R., Stewart, G., Fergason, S., Curtiss, T., and Seibold, R., "Causes and Mitigation of Radio Frequency (RF) Blackout During Reentry of Reusable Launch Vehicles," El Segundo Aerospace Rept. ATR-2007(5309)-1, 2007.

[3] Kim, M. K., "Electromagnetic Manipulation of Plasma Layer for Re-Entry Blackout Mitigation," Ph.D. Dissertation, Univ. of Michigan, Ann Arbor, MI, 2009.

[4] Sgobba, T., "A Space Debris Alert System for Aviation," *6th IAASS Conference*, Montreal, Canada, 2012.

[5] Azriel, M., "European Space Agency Files Patent for Debris Alert System," *Space Safety Magazine*, European Space Agency, Dec. 2012, http://www.spacesafetymagazine.com/media-entertainment/european-space-agency-files-patent-debris-alert-system/ [retrieved 1 Dec. 2015].

[6] Emanuelli, M., and Sgobba, T., "Assessing the Aviation Risk from Space Debris and Meteoroids," *Space Safety Magazine*, Summer, No. 8, 2013, pp. 24–25.

[7] Bonacina, F., "Lessons Learnt from Beagle 2 and Plans to Implement Recommendations from the Commission of Inquiry" [online publication], ESA, Ireland, May 2004, http://www.esa.int/ESA_in_your_country/Ireland/Lessons_learnt_from_Beagle_2_and_plans_to_implement_recommendations_from_the_Commission_of_Inquiry [retrieved 26 Jan. 2014].

[8] Krebs, G., "QARMAN (QB50 BE05)," Gunter's Space Page [online database], Aug. 2015, http://space.skyrocket.de/doc_sdat/qarman.htm [retrieved 1 Dec. 2015].

[9] Rybak, J. P., "Causes, Effects, and Diagnostic Measurements of the Reentry Plasma Sheath," Colorado State Univ. AFCRL-70-0707, Fort Collins, CO, 1970.

[10] Morabito, D., "The Spacecraft Communications Blackout Problem Encountered During Passage or Entry of Planetary Atmospheres," California Inst. of Technology, Jet Propulsion Lab. Rept. 42-150, Pasadena, CA, 2002.

[11] Spencer, D. F., "An Evaulation of the Communication Blackout Problem for a Blunt Mars-Entry Capsule and a Potential Method for the Elimination of Blackout," California Inst. of Technology, Jet Propulsion Lab. Rept. 32-594, Pasadena, CA, 1964.

[12] Reynier, P., and Evans, D., "Postflight Analysis of Inflatable Reentry and Descent Technology Blackout During Earth Reentry," *Journal of Spacecraft and Rockets*, Vol. 46, No. 4, 2009, pp. 800–809. doi:10.2514/1.41480

[13] Greendyke, R. B., Gnoffo, P. A., and Lawrence, R. W., "Calculated Electron Number Density Profiles for the Aeroassist Flight Experiment," *Journal of Spacecraft and Rockets*, Vol. 29, No. 5, 1992, p. 621–626.

[14] Dunn, M. G., and Kang, S.-W., *Theoretical and Experimental Studies of Reentry Plasmas*, NASA CR-2232, Washington, D.C., 1973.

[15] Park, C., "A Review of Reaction Rates in High Temperature Air," *24th Thermophysics Conference*, June 1989.

[16] Park, C., "Nonequilibrium Hypersonic Aerothermodynamics," Wiley, New York, 1990.

[17] Savino, R., Paterna, D., and De Stefano, M., "Plasma-Radiofrequency Interactions Around Atmospheric Re-Entry Vehicles: Modeling and Arc-Jet Simulation," *Open Aerospace Engineering Journal*, Vol. 3, No. 1, 2010, pp. 76–85.

[18] Steiger, M. H., Leslie, G., Fernandez, F. L., and Fedele, J. B., "Reentry Communication: Theoretical Analysis and Flight Test Results," AIAA Paper 1970-0220, 1970.

[19] Lew, H. G., "Angle-of-Attack Effects on Electron Density Distribution Over Blunt Bodies," National Technical Information Service, U.S Dept. of Commerce, AFCRL CR-74-0354, Massachusetts, 1974.

[20 Storelli, A., "Assessment of Phoebus Reentry Blackout," European Space Research and Technology Centre (ESTEC), Thesis Final Report, Noordwijk, The Netherlands, 2011.

[21] Walter Vincenti, C. K., *Introduction to Physical Gas Dynamics*, Krieger, Huntington, NY, 1967, pp. 132–135.

[22] Panesi, M., Magin, T., Bourdon, A., Bultel, A., and Chazot, O., "Analysis of the FIRE II Flight Experiment by Means of a Collisional Radiative Model," *Journal of Thermophysics and Heat Transfer*, Vol. 23, No. 2, 2009, pp. 236–248.

[23] "CFD++ Chemistry Options," Metacomp Technologies Inc., Agoura Hills, CA, 2013, http://www.metacomptech.com/index.php/products/cfd/chemistry [accessed 18 Dec. 2013].

[24] Anderson, J. D., *Hypersonic and High Temperature Gas Dynamics*, McGraw–Hill, New York, 1989, pp. 610–652.

[25] Mitchner, M., and Kruger, C. H., *Partially Ionized Gases*, Wiley, New York, 1973, pp. 155–161.

[26] Takahashi, Y., Yamada, K., and Abe, T., "Prediction Performance of Blackout and Plasma Attenuation in Atmospheric Reentry Demonstrator Mission," *Journal of Spacecraft and Rockets*, Vol. 51, No. 6, 2014, pp. 1954–1964. doi:10.2514/1.A32880

[27] Brown, L., Fischer, C., Boyce, R. R., Reinartz, B., and Oliver, H., "Computational Studies of the Effect of Wall Temperature on Hypersonic Shock-Induced Boundary Layer Separation," *Shock Waves: 26th International Symposium on Shock Waves*, Vol. 2, Pt. 19, 2009, pp. 1231–1236.

[28] "A Sample Atmosphere Table (SI Units)" [online database], Public Domain Aeronautical Software, Santa Cruz, CA, http://www.pdas.com/atmosTable1SI.html [retrieved Sept. 2013].

[29] "CFD + + User Manual," Metacomp Technologies Inc., Agoura Hills, CA, 2013, http://metacomptech.com/outgoing/training/cfdppmanual.pdf [accessed 5 Dec. 2013].

[30] Barbante, P. F., "Accurate and Efficient Modelling of High Temperature Nonequilibrium Air Flows," Ph.D. Dissertation, von Kármán Inst., Rhode-Sint-Genise, Belgium, 2001.

[31] Quanhua, S., Huiyu, Z., Wang, G., and Jing, F., "Effects of Mesh Resolution on Hypersonic Heating Prediction," *Theoretical and Applied Mechanics Letters*, Vol. 1, No. 2, 2011, p. 1–4.

[32] Farbar, E. D., Boyd, I. D., and Martin, A., "Modeling Ablation of Charring Heat Shield Materials For Non-Continuum Hypersonic Flow," *50th AIAA Aerospace Sciences Meeting Including the New Horizon Forum and Aerospace Exposition*, AIAA Paper 2012-0532, 2012.